Full Length Article

Analysis of the role of the pH in the anchoring of alkylphosphonic acid on a TiO$_2$ surface: A DFTB study

Daniele Veclani [a],[*], Andrea Melchior [b], Antoni Llobet [c], Nicola Armaroli [a], Alessandro Venturini [a],[*]

[a] Istituto ISOF, Consiglio Nazionale delle Ricerche, 40129 Bologna, Italy
[b] Dipartimento Politecnico di Ingegneria e Architettura (DPIA), Laboratori di Chimica, Università di Udine, 33100 Udine, Italy
[c] Institute of Chemical Research of Catalonia, ICIQ, Avinguda Paisos Catalans 16, E-43007 Tarragona, Spain

ARTICLE INFO

ABSTRACT

The reactivity of a (1 1 0) rutile titanium dioxide surface functionalized with neutral, anionic and di-anionic forms of dodecyl-phosphonic acid was studied by Density Functional based Tight Binding theory to simulate different pH conditions. Functionalization of this surface is relevant for at least two reasons: a) to protect the surface against external agents (e.g., by preventing the proliferation of bacteria in medical implants) and b) to use these organic–inorganic hybrid materials to facilitate the anchoring of other molecules. Comparing the results obtained in the gas phase and in water, experimental findings are better modelled by considering the hydration energy of the acids and the solvation-desolvation process involving the acids and the surface. In water, in all protonation states, acid molecules interact with the hydrated surface as a mono-negative charged species due to proton transfer before the grafting process. The formation of bi-dentate, di-anionic acid species, due to a proton transfer process or a change of pH, is favoured by anchoring alkylphosphonic acid to the rutile.

1. Introduction

Biomaterials are defined as materials able to interact with biological organisms, which can be used to test, treat or replace organ tissues [1,2]. The ideal properties of a biomaterial include: a) no immune response; b) integration with a particular tissue or cell; c) no toxicity; d) low allergic response; e) corrosion resistance [2].

Among all possible materials able to interact with fluids and human tissues (metals, polymer, ceramic and natural materials) [1,3], metals play a predominant role. It is estimated that ~70% of the implanted surgical devices are characterized by metal-based biomaterials [4]. One of the most used metals in the production of medical devices is titanium and its alloys. Some peculiar proprieties such as good corrosion resistance, low density and weight, optimal biocompatibility and low Young`s modulus make them preferable to other metals (e.g., chromium–cobalt alloys and stainless steel) [5,6]. Titanium biomaterials are used in dental implants [6], screws and clips in bone fixation [7,8], artificial heart valves [9,10], and joint implant devices [3]. On the other hand, despite the excellent properties of titanium and its oxide biomaterials, the risk of implant failure, largely due to bacterial infections,

is higher without implant surface modification [11].

Different surface treatment strategies could be used in order to improve the performance of biomaterials in biological systems, such as: mechanical, physical and chemical methods [12,13].

Chemical and biochemical methods, including surface coating with organic molecules [11], antibacterial metal [14], antimicrobial peptides [15], antibiotics [16] and antibacterial macromolecules [17], are some of the most used strategies to prevent bacterial attack.

Among them, organic molecules like catechol [18], silanes [19,20], carboxylic acids [21] and phosphates-phosphonates or they organo-derivatives are grafted to the TiO$_2$ surface to form stable and well-defined self-assembled monolayers (SAMs) [22]. The presence of suitably modified organic molecules together with formation of SAMs allows the formation of covalent (antimicrobial peptide [23], polymers [18,24], cyclodextrin [25]), dative bond (metals cation [26]) or non-covalent interactions [27].

Organophosphonic acids (OPAs), one of the most used grafting molecules, have some advantages over other molecules because of a greater hydrolytic stability in water environment [28]. Moreover, surface acid treatment is not required to obtain high coverage when OPAs

* Corresponding authors.
E-mail addresses: daniele.veclani@isof.cnr.it (D. Veclani), alessandro.venturini@isof.cnr.it (A. Venturini).

are used [29]. For these reasons, interactions between TiO$_2$ surface and OPAs were extensively studied both experimentally [30–41] and theoretically [42–49].

Experimental results indicate that the formation of M—O—P (Tì—O—P) bonds occurs through condensation reactions between the surface M—O—M groups and the OPAs P—OH moieties. Moreover, the Lewis acid sites of the surface can be coordinated by phosphoryl oxygen [40]. Despite many experimental studies [30–41] that have been reported over the past decade, the rationalization of the coordination of OPAs to the TiO$_2$ surface have proved unsatisfactory. Solid state ^{31}P NMR and infrared spectroscopy (IR) studies indicate that different coordination modes such as mono- (μ_1), μ_2-bridging bi-dentate (μ_2) and μ_3-bridging tri-dentate (μ_3) structures are possible (Fig. 1) [35,46].

Some works reported greater stability of the tri-dentate species [34,39], while others of bi-dentate ones [22,36,37]. In a recent work, Canepa *et al.* studied the anchoring of aminophosphonates on the TiO$_2$ surface by using X-ray Photoelectron Spectroscopy (XPS) and IR techniques [22]. The XPS results indicate that mono-dentate and bi-dentate coordination modes are predominant with respect to the tri-dentate.

Isothermal titration calorimetry (ITC) study made to obtain the reaction enthalpies ($\triangle H_r$) show that the interaction between three different OPAs (Methylphosphonic, *n*-octylphosphonic and *n*-octadecylphosphonic acid) and TiO$_2$ surface favors the reaction of short alkyl chains (methylphosphonic, *n*-octylphosphonic acid) compared to long alkyl chains (*n*-octadecylphosphonic acid). However, dissociation energy (E$_{diss}$) values were stabilizing by 13.9 ± 2 kcal•mol^{-1} [38].

The free energy of binding between TiO$_2$ surface and some OPAs obtained by thermogravimetric (TGA) analysis were negative and close to -5 kcal•mol^{-1} for hexylphosphonic, hexadecylphosphonic and phenylphosphonic acids [30].

Much computational work has been done to model the available and non-conclusive experimental data on OPAs adsorption [42–49]. In previous works, Density Functional Theory (DFT) calculations have been extensively used [42–49]. In particular, Projector Augmented Wave (PAW) method, for basis set, together with generalized gradient approximation (GGA) functionals, such as PBE [42,46–48] and PW91 [43], are some of the most used level of theory. However, B3LYP hybrid functional with Gaussian type orbital (GTO) are also reported [44,48]. In these works [42–49] the interaction energy (IE) between OPAs and

TiO$_2$ surface, in the gas phase, is in the range between -40.0 and -80.0 kcal•mol^{-1}. For example, Di Valentin and co-workers [47] studied the relationship between surface covering levels and the interaction of *n*-butylphosphonic acid on the anatase surface. The bidentate mode, together with the mono-dissociation of the acid (proton transfer from acid to surface) is preferred at low coverage levels. At high coverage levels, monodentate coordination is the most stable, with the acid changing its conformation in order to minimize lateral repulsions.

Quintero *et al.* studied the dissociative adsorption of dimethyl methyl phosphonate, sarin and soman toxic agents on dry and wet rutile surfaces [42]. This work introduces the concept of wet condition, when the surface is covered with water film. This effect is useful to partially reproduce the influence of the solvent. In their work the authors obtain this condition using both a hydrated and a hydroxylated water configuration.

The results indicate that, for both conditions, dissociative adsorption (proton transfer from acid to surface) is preferred over molecular adsorption. Moreover, higher stability was observed when a hydrated surface was employed. A similar protocol was recently used to study the interaction between aminopropylphosphonic acid and mesoporous TiO$_2$ powder [46].

Several limitations of these computational studies need to be emphasized:

(a) The interactions between the surface and anionic species of OPAs, which predominate at physiological pH, have not been studied [41].
(b) The formation of the tri-coordinated structures is reported only in one case where a nanosized polyoxotitanate cluster instead of TiO$_2$ surface was employed [50].
(c) The contribution of the explicit solvent was never considered.
(d) The coordination mode depends on another important factor, *i.e.* the pH [36,41]. Indeed, by increasing the pH value, deprotonation of the OPA is observed with the formation of two anionic species, mono-anionic and di-anionic. On the other hand, the presence of explicit solvent is essential because the solute–solvent interactions are responsible for the significant changes in the chemical and physical characteristics of organic dyes, OLEDs and energetic materials among others [51–53].

Mono-coordinated structures
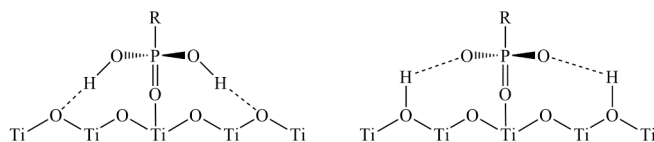
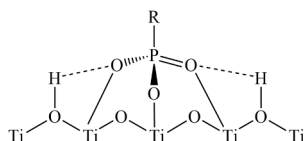## Bi-coordinated structures
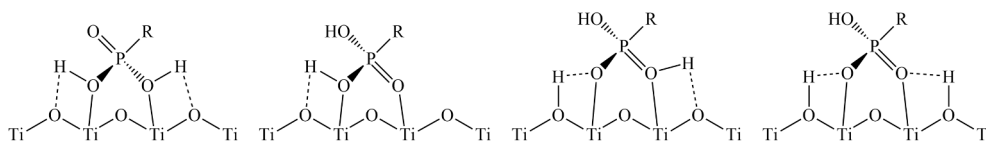
Tri-coordinated structure

Fig. 1. Possible binding mode for neutral forms of OPAs: a) µ1-bridging mono-dentate; b) µ2-bridging bi-dentate; c) µ3-bridging tri-dentate structures.

Here we describe a computational study that allows to elucidate the nature of the interactions between the (1 1 0) TiO$_2$ rutile surface and *n*-dodecyl-phosphonic acid (C12-PA) as a function of pH. This has been done in the presence of explicit water molecules and by comparing the results with the corresponding gas phase study. We use the self-consistent-charge density functional tight-binding (SCC-DFTB) method [54,55]. This DFT approximated method, reduces the computational demand making it 2–3 orders of magnitude faster than standard DFT without any significant loss of accuracy [56]. In particular, with this method, nanoparticles or large slab of TiO$_2$, together with their interactions with water [57–59], organic molecules [45,60,61] or biomolecules [62] were investigated.

2. Experimental

2.1. SCC-DFTB method

The approximation of the Kohn-Sham (KS) DFT formalism is the basis of the self-consistent charge density-functional-based tight-binding (SCC-DFTB) method. This approximation assumes a second-order expansion of the KS-DFT total energy with respect to the electron density fluctuations. The SCC-DFTB total energy is defined in equation (1) [58]:

$$E_{tot}^{SCC-DTFB} = \sum_i n_i \varepsilon_i + \frac{1}{2}\sum_{\alpha\beta} v_{rep}^{\alpha\beta}(R_{\alpha\beta}) + \frac{1}{2}\sum_{\alpha\beta}\gamma_{\alpha\beta}\Delta q_\alpha \Delta q_\beta \quad (1)$$

the attractive part of the energy, represented by the first term, contains the one-electron energies ε_i from the diagonalization of an approximated Hamiltonian; the short-range repulsive energy, approximated in the second term, is represented by the sum of the pairwise distance-dependent potential $v_{rep}^{\alpha\beta}(R_{\alpha\beta})$ between the pair of atoms α and β; $\triangle q_\alpha$ and $\triangle q_\beta$ are the charges induced on the atoms α and β, which interact through a Coulombic-like potential $\gamma_{\alpha\beta}$. All SCC-DFTB calculations were carried out with the DFTB+ software [63].

2.2. Geometry optimization procedure

All geometry optimizations were carried out with the use of "matsci-0–3" Slater–Koster parameters specifically designed for material science [64]. Matsci is appropriate for the study of the interaction of TiO$_2$ surface and phosphonic acid [45,60].

The quasi-Newton optimization method (Limited memory BFGS optimizer) was employed; the self-consistent tolerance was set to 10^{-5} electrons. The k-point set for the Brillouin-zone integration were $2 \times 2 \times 1$ as already used [58,59]. The highest angular momentum was set as "s" for hydrogen atoms, "p" for oxygen and carbon atoms and "d" for phosphorus and titanium atoms. The van der Waals interactions have been corrected with the use of DFT-D4 method [65]. Periodic boundary conditions were applied in all directions.

2.3. Model

The 110 surface of TiO$_2$ rutile is the most stable and therefore the most studied one [66]. For the gas-phase calculations, it was built a (1 1 0) rutile 5×3 slab structure corresponding to a 14.849×19.735 Å^2 surface area with 4 rutile layers (Fig. 2a-b). Moreover, a vacuum region of $14.849 \times 19.735 \times 36.1$ Å^3 volume was added.

For this study we use the *n*-dodecyl-phosphonic acid (C12-PA, Fig. 2c-e), which is able to create the most stable SAMs both in air and in solvent [47]. To mimic the modification of the pH of the solution three forms of dodecyl-phosphonic acid i.e., neutral (C12-PA), anionic (C12-PA$^-$) and di-anionic (C12-PA^{2-}) were used (Fig. 2c-e).

The geometry optimization in the gas-phase started with the C12-PA molecule placed on top of the rutile (1 1 0) surface. This cluster presented one C12-PA molecule per 15 5-coordinated Ti (Ti$_{5c}$) atoms.

Mono, μ$_2$-bridging bi-dentate and μ$_3$-bridging tri-dentate coordination mode of the C12-PA was used as starting configurations. The interaction energy in the gas-phase (IE$_{Gas}$) was calculated following equation (2):

$$IE_{Gas} = E_{cluster} - (E_{surface} + E_{C12-PA}) \quad (2)$$

where E$_{cluster}$ is the energy of the C12-PA anchored on the rutile (1 1 0) surface, E$_{surface}$ corresponds to the energy of the clean rutile (1 1 0) surface and E$_{C12-PA}$ is the energy of an isolated C12-PA molecule.

To study the C12-PA adsorption at the solid-solution interface, the empty part of the simulation box was filled with 249 water molecules. The starting configurations were obtained by molecular dynamics (MD) simulations. The simulations were carried out in the NVT ensemble. Temperature was kept constant by applying the Nose-Hoover thermostat [67] at 300 K. NVT molecular dynamic simulations of 5 ps, with the TiO$_2$ surface atoms positions kept constant were carried out. These molecular dynamics simulations were used to equilibrate the water molecules and C12-PA, which were
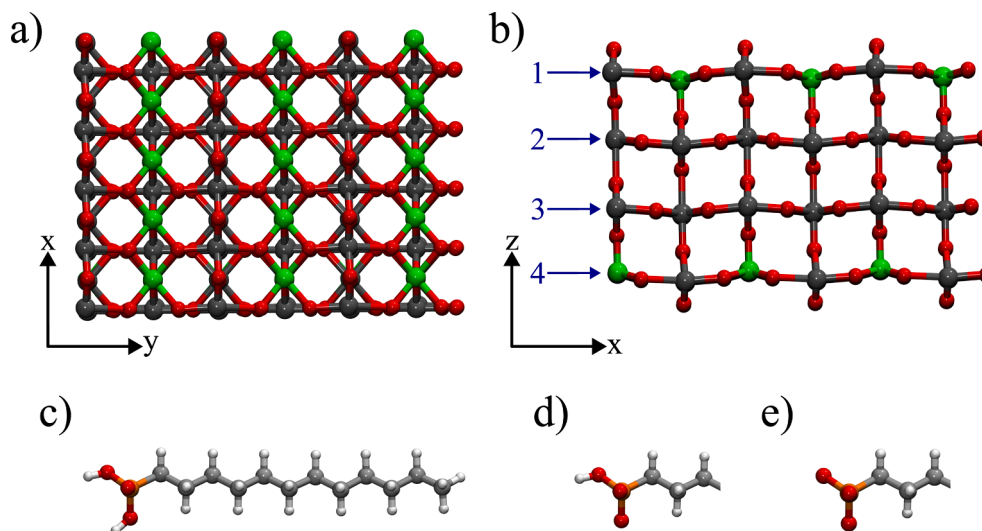
Fig. 2. Model employed in this work: a) rutile (1 1 0) along the xy axis; b) rutile (1 1 0) along the xz axis with the identification of the four layers. Five coordinate Ti (Ti5c) atoms highlighted in green. 3 forms of *n*-dodecyl-phosphonic acid (C12-PA) model used in this work: c) neutral form; d) anionic form (charge −1) and e) di-anionic (charge −2). (For interpretation of the references to colour in this figure legend, the reader is referred to the web version of this article.)

subsequently optimized with the procedure reported above.

The interaction energy in water (IE_{w_1}) was calculated by means of equation (3):-

$$IE_{w\_1} = E_{cluster} - \left(E_{surface-w} + E_{C12-PA}\right) \tag{3}$$

where $E_{cluster}$ is the energy of C12-PA anchored on the solvated rutile (1 1 0) surface, $E_{surface-w}$ corresponds to the energy of the solvated clean rutile (1 1 0) surface and E_{C12-PA} is the gas-phase energy of an isolated C12-PA molecule. In a similar way Quintero et. al. have calculated the interaction between the wet rutile surface and nerve agents [42]. This approach does not take into account the energy contribution related to the solvation of the acid molecules and the surface. The IE_{w_2} in the solvent was then calculated according to equation (4):

$$IE_{w\_2} = E_{cluster} - E_{sur\_acid\_non\_inter} \tag{4}$$

where $E_{cluster}$ is the energy of C12-PA anchored on the rutile (1 1 0) surface in a solvated box, $E_{sur\_acid\_non\_inter}$ corresponds to the energy of acid molecules placed at ~ 6 Å from the surface, in a solvated box and not interacting with the surface after an optimization procedure (Fig. S1 in the supporting information (SI)).

Finally, optimization of 249 water molecules and the acid (without the surface) allowed to obtain the hydration energy of C12-PA (E_{hyd}) following equation (5):

$$E_{hyd} = E_{acid\_w} - \left(E_{acid\_gas} + E_{w}\right) \tag{5}$$

where E_{acid_w} is the energy of acid immersed in a box of 249 water molecules, E_{acid_gas} corresponds to the energy of acid in gas-phase and IE_w is the energy of a box of 249 water molecules.

3. Results and discussion

As reported above, to consider the pH of the solution, we have studied the addition of the three C12-PA molecules (Fig. 2c-e) onto rutile (1 1 0) surface in gas phase and in explicit water.

Clearly, variations in the strength of these bonding modes depends on:

a) how many phosphoryl oxygens coordinate the surface;
b) how many hydrogen bonds are formed between the acid molecule and the oxygen of the surface (before the proton transfer);
c) how many hydrogen bonds are present, following proton transfer between acid and surface.

We initially discuss the interaction in the gas-phase, followed by the discussion of the interaction in explicit water and finally we briefly analyze the electronic properties. The reader is referred to the SI for additional numeric results and structural data.

3.1. Gas phase

In Fig. 3 the energy profile for the addition of the three acid structures (Fig. 2c-e) to the rutile TiO_2 surface in gas phase is shown (Table S1 and all geometric details in Table S2-S5 and Figure S2).

Our description of the energy profile, related to each individual C12-PA molecule (neutral, anionic and di-anionic) follows the formation of the M−−−O—P bonds. To simplify the description of this mechanism, we have divided the energy profile in the following steps where, for each step, the most stable structure detected is indicated:

(a) Step 1: System A, with one M−−−O—P bond;
(b) Step 2: System B, with two M−−−O—P bonds;
(c) Step 3: System C, with two M−−−O—P bonds and one proton transfer from the acid to the surface;
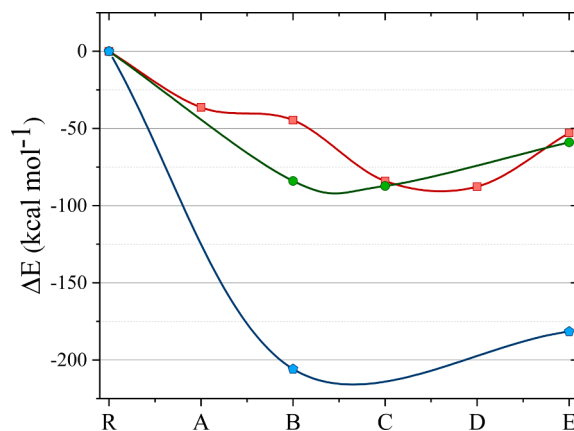

Fig. 3. IE_{Gas} profiles of the three C12-PA species in gas phase for neutral form of C12 PA (red line); anionic C12-PA (green line); and di-anionic C12-PA (blue line). The lines between the points are only provided to facilitate visualization. (For interpretation of the references to colour in this figure legend, the reader is referred to the web version of this article.)

(d) Step 4: System D, with two M−−−O—P bonds and two proton transfers from the acid to the surface;
(e) Step 5: System E with three M−−−O—P bonds.

Neutral C12-PA (red line in Fig. 3*, structures in* Fig. 4*, ng):* in the gas phase, the energy profile of the neutral acid consists of five steps. The negative IE_{Gas} energies indicate a favorable interaction between C12-PA
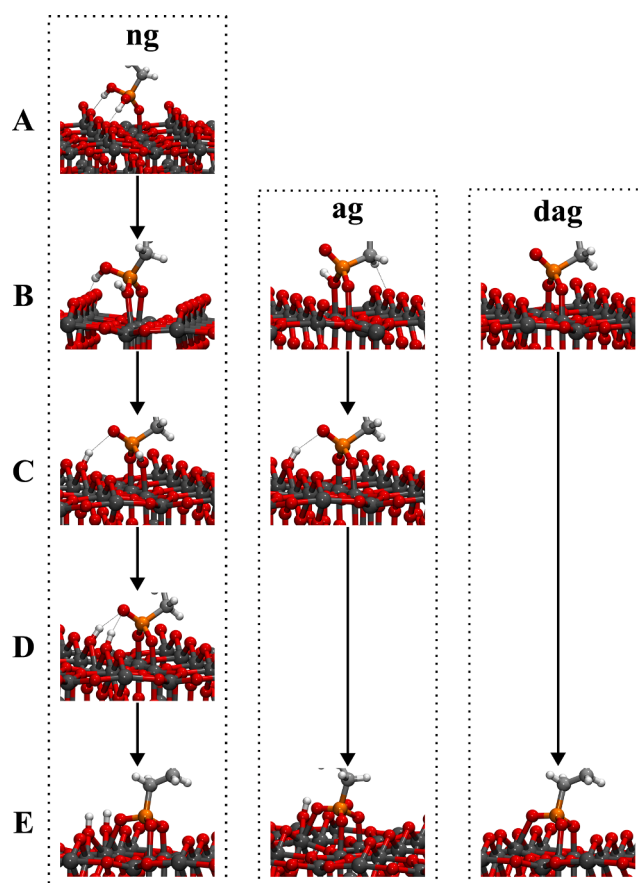

Fig. 4. Optimized structures for the anchoring of C12-PA to the rutile (1 1 0) surface; Step A: mono-coordinated structures; Step-B: bi-coordinated structures; Step C: first proton transfer (PT); Step D: second PT; Step E: tri-coordinated species; ng: neutral-gas; ag: anionic-gas; dag: di-anionic-gas.

and the surface. In mono-coordinated structures A (Fig. 4), P=O oxygen (=O) interacts with Ti atom through a dative bond with a distance (Ti–O_{C12-PA}) of 2.258 Å (Table S2 and Figure S2). Angle Ti_{1L}-Ti_{1L}-O_{C12-PA} (Table S3 and Figure S2), which indicates the tilt of the oxygen acid atoms coordinated with the surface, is 86°. The IE_{Gas} is −36.3 kcal•mol^{-1} and the stabilization are in part due to the two hydrogen bonds (H-bond) that the acid forms with two oxygen atoms of the surface (Fig. 4 Ang). In the second step, the formation of another Ti—O bond, to form the bi-coordinated structure **B,** was reported (Fig. 4 Bng). Ti–O_{C12-PA} distances were slightly higher in comparison with structure **A** (2.291 and 2.261 Å, Table S2) while the Ti_{1L}-Ti_{1L}-P-O_{C12-PA} angles present different values (82° and 95° Table S3, and Figure S2) indicating a distortion of the two Ti—O_{C12-PA} bonds. The IE_{Gas} was −44.6 kcal•mol^{-1} with a stabilization of the system by −8.3 kcal•mol^{-1} even though the system loses one H-Bond with the surface (Fig. 4 Bng). Similar trend was previously reported in literature for acid molecules at low coverage level [47].

In structure **C** (Fig. 4, Cng) the first proton transfer process (PT) occurs with a consequent decrease of one Ti—O_{C12-PA} distance (Table S2), the Ti_{1L}-Ti_{1L}-P-OC_{12-PA} angle value was similar and close to 90° (Table S3). This process introduces a deformation in the surface with an increase in the Ti—O bond (Table S2 and Figure S2) implicated in the proton transfer. The transferred hydrogen remains bound to the acid through a H-bond (Fig. 4 Cng). The PT process stabilizes the system by ∼ 40 kcalfmol^{-1} (Fig. 3 ng and Table S1) in comparison with the bi-coordinated structure **B**. The second PT in structure **D** (Fig. 4 Dng) shows an additional decrease in Ti—O_{C12-PA} distances (Table S2) and the IE_{Gas} value shows a slight stabilization compared to structure **C** (∼3 kcal•mol^{-1}; Fig. 3 ng and Table S1). The two transferred hydrogens interact with acid by H-bonds (Fig. 4 Dng).

The tri-coordinated structure **E** (Fig. 4, Eng), was obtained with an increase in all the Ti—O_{C12-PA} distances (Table S2) with the third bond which is the longest (Table S2) and with higher Ti_{1L}-Ti_{1L}-P-O_{C12-PA} angle values (Table S3). The formation of the third bond induces a deformation of the surface, the Ti_{6c} atom, involved in the third bond, forms a O—Ti—O angle (167° see Figure S2) which is lower if compared to the atoms not involved in the formation of the bonds with acid (Ti_{5c} ∼ 170°). Moreover, this bond, induces a deformation also in acid molecule; the Ti_{2L}-P-O_{C12-PA} angle (Table S3 and Figure S2), which indicates the tilt of the alkyl acid chain towards the surface, increases with respect to mono and bi-coordinated structures. The structural deformation of the surface discussed above could explain the destabilization observed for structure **E** (+34.8 kcal•mol^{-1} in respect to structure **D**).

In other words, despite the increase in number of the Ti—O—P-bonds the system is less stabilized. Consequently, the grafting reaction stops at structure **D**ng with the tri-coordinate species **E**ng (Fig. 4) that could be formed only in small amounts. This result is in good agreement with experimental data [22].

Anionic C12-PA (green line in Fig. 3, *structures in* Fig. 4, *ag):* In the case of the anionic acid, the mono-coordinated structure **A** was not observed and the presence of a nucleophilic O⁻ group could explain this behavior. The first detected system is **B** (Fig. 4 ag) characterized by similar distances, angles and IE_{Gas} values observed for structure **C**ng (Table S2 and S3). The anionic **B**ag structure interacts more strongly with the surface compared to the neutral **B**ng. Analogous to structure **B**ag, structure **C**ag was characterized by similar distances, angles, and IE_{Gas} value observed for structure **D**ng.

Again, the tri-coordinated structure **E**ag shows similar behavior in the geometrical parameters trend observed for **E**ng, but with a slightly lower IE_{Gas} value (-59.0 kcal•mol^{-1} Table S1) and consequently shows lower destabilization (+28.3 kcal•mol^{-1} Table S1) in comparison with structure **C**ag (for ng +34.8 kcal•mol^{-1} Table S1).

Di-anionic C12-PA (blue dashed line in Fig. 3, *structures in* Fig. 4, *dag):* The absence of –OH groups in C12-PA^{2-} implies the formation of only two structures, bi-coordinated (**B**) and tri-coordinated (**E**), reported in Fig. 4. Structure **B**dag which is characterized by the most negative IE_{Gas}

value (table S1) shows geometrical parameters similar to those observed for the structures **C**ag and **D**ng (Table S2 and S3). The presence of two negative oxygen atoms makes this molecule highly nucleophilic and capable of a very strong interaction with the surface. Similarly, tri-coordinated structure **E**dag (Fig. 4ag), was destabilized in energy by +24.2 kcal•mol^{-1}, in comparison with structure **B**dag, nevertheless, **E**dag is more stable than **E**ng (by +34.8 kcal•mol^{-1}) and **E**ag (by +28.3 kcal•mol^{-1}).

In summary, in the gas phase, all calculated IE_{Gas} were negative indicating a favorable interaction between surface and the three different acid species. The analysis of the IE_{Gas} profile for C12-PA indicates that the most stable conformations follow the order: dag > ag ≈ ng (Fig. 3 and Table S1). It is interesting to note that the formation of a mono or di-anionic acid species, due to a PT process or to a change in pH, seems to be the driving force relative to the formation of the interaction between the TiO_2 (1 1 0) rutile surface and acid.

3.2. Water phase

In Figure S3 it has been reported the optimized structure of the interacting water molecules with the clean surface. The first water layer was constituted by water molecules that interact with the surface through the formation of a bond between the oxygen atoms of water (O_w) and Ti_{5c} atoms (labelled Ti—O_w). The calculated average distance, from optimized structures, between adsorbed waters (O_w) and Ti_{5c} atoms (Ti—O_w^{ay}) is 2.292 Å. A second water layer interacts through H-bonds (average distance of 1.808 Å) with the first one.

The obtained gas-phase structures were subsequently solvated and re-optimized (Figure S4) after NVT simulations, the bond length and angles are close to those observed for gas-phase calculations (Table S4 and S5).

IE_{w_1} values are close to those obtained in the gas-phase (Table S1 IE_{Gas} *vs* IE_{w_1}). On the other hand, IE_{w_1} values, do not consider the hydration energy (E_{hyd}) of the acid (from gas-phase to solvent) which is usually a not negligible contribution [68], together with the desolvation process related to the anchoring. The E_{hyd} values obtained decrease in this direction: neutral > anionic > di-anionic (-26.5, −119.6 and −263.3 kcal•mol^{-1} respectively).

During the anchoring of the acid on the surface, a desolvation of both acid and the surface is observed, evidenced by the decrease in the number of solvent molecules surrounding the acid and surface (N_{w_acid} and N_{w_sur} in Table S1).

The strong stabilization of the three acid molecules, due to their E_{hyd}, and the solvation-desolvation process, changes drastically the energy profile as highlighted by IE_{w_2} values (see Fig. 5 and Table S1) and most of the systems grafted onto the surface are now strongly destabilized.

A better description of the anchoring process requires to take into account at least one structure where acid does not interact directly with the TiO_2 but interact with coordinated surface waters (**HB** in Fig. 6).

Neutral C12-PA (red dot and solid lines in Fig. 5 *and* Fig. S4, *nw):* The energy profile in water starts with the stable structure **HB**nw (-10.1 kcal•mol^{-1}) where two hydrogens are transferred to the surface but, at the same time, the acid molecule removes a hydrogen from the coordinated water (Fig. 6, **HB**nw). The intermediates **A**nw, **B**nw and **C**nw (red dashed line Fig. 5, see also Figure S4) are unlikely because of the destabilizing IE_{w_2} values (73.1, 40.3 and 10.3 kcal•mol^{-1} respectively). Instead, the **D**nw bi-dentate system has a stabilization energy comparable with that of **HB**nw (Table S1) indicating that the two structures could coexist (Table S1).

Anionic C12-PA (green lines in Fig. 5, Fig. S4, *aw):* the first **HB**aw structure is −3.6 kcal•mol^{-1} (IE_{w_2}) more stable than the reactants and shows similar behavior observed for the neutral form; a proton transfer process from acid to surface and from surface to acid (Fig. 6 **HB**aw). In these pH conditions, the only stable structure is the **C**aw (IE_{w_2} −19.2 kcal•mol^{-1}). Due their energy destabilization systems **A**aw, **B**aw and **E**aw are not formed.
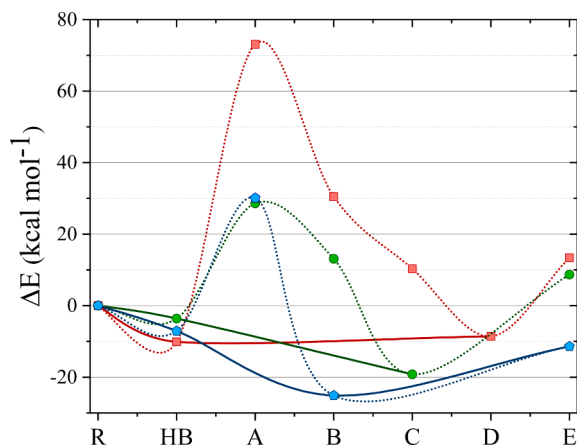
Fig. 5. IE$_{w\_2}$ profiles of the three C12-PA species in water for neutral form of C12 PA (red line); anionic C12-PA (green line); and di-anionic C12-PA (blue line). IE$_{w\_2}$ profiles with the destabilized structures for comparison are reported (dotted lines). The lines between the points are only provided to facilitate visualization and do not imply the actual pathway of the reaction. (For interpretation of the references to colour in this figure legend, the reader is referred to the web version of this article.)

Di-anionic C12-PA (blu lines in Fig. 5 *and* Fig. S4, *daw):* in basic conditions the **HB**daw structure is stable (IE$_{w\_2}$ −7.1 kcal•mol^{-1}) and shows a PT transfer from the surface coordinated water to the acid (Fig. 6 **HB**daw). At this pH, bi-coordinated **C**daw structure and tri-coordinated **E**daw structure are stable (IE$_{w\_2}$ −25.1 and −11.4 kcal•mol^{-1} respectively, Table S1).

In conclusion, in water, all three acid species show stable structures in which the acid moieties are not directly bound to the surface but interact with the water molecules coordinated to the surface (Fig. 6). Neutral and anionic acid systems exhibit only one stable structure directly grafted to the surface: bi-coordinated **D**nw in neutral conditions and bi-coordinated **C**aw in slight acid conditions, where a mono- or di-dissociative state structure is observed. In basic conditions, di-anionic acid shows two structures directly grafted to the surface, *i.e.*, bi-dentate **C**daw and tri-dentate **E**daw.

The IE$_{w\_2}$ value, are now close to those reported experimentally [38]. These experimental works suggest specific interactions of the acid with the surface thanks to the formation of P—O—M bonds or to the formation of multiple H-bonds [38]. Moreover, in these experiments, it is concluded that, depending on whether the alkyl chains are short (C$_8$) or long (C$_{18}$), the binding mode is exothermic or endothermic, respectively. This suggest that in long-chained acids, the grafting process is entropy driven [38]. Our calculations, which show the decrement in the number of water molecules around the anchored acid structure (N$_{w\_acid}$ and N$_{w\_sur}$, in Table S1), confirm this behavior for long alkyl chains OPAs.

3.3. Electronic structure analysis

The electronic properties of a metal oxide with a relatively large band gap (BGs), such as TiO$_2$ (3.1 eV for rutile [69]), are difficult to describe by DFT calculations. GGA DFT functionals, underestimate the band gap value, whereas hybrid DFT functionals provide better results [70,71]. On the other hand, SCC-DFTB calculations were only used for bulk TiO$_2$ simulations and the calculated BG are in excellent agreement with experimental data [72]. Density of state (DOS) are reported in Figure S5 and S6 (gas-phase and in water respectively). As previously reported in literature [46,47], no additional gap states were introduced by anchoring of C12-PA molecules. No additional gap states were observed after the PT processes or after the formation of the tri-coordinated structures. The BG values, reported in Table S1, were close to ~3.00 eV in excellent agreement with experimental results for clean surfaces [69].

4. Conclusions

We have used DFTB method to assess the anchoring ability of the *n*-dodecyl-phosphonic acid on rutile (1 1 0) surface. Three different acid species – neutral, anionic and di-anionic – have been considered to evaluate the impact of pH in the grafting process.

Our simulations in the gas-phase support a favorable interaction between different acid species and surface in all the cases studied, as highlighted by negative IE$_{Gas}$ values. The analysis of the energy profile indicates that neutral and anionic acids are characterized by similar energy values and the most stable conformations were bi-dentate structures (mono or di-dissociated state).

Moving towards basic conditions, anchored di-anionic and bi-dentate structures are the most stable over neutral and anionic acid forms. All the tri-coordinated systems are destabilized compared to the bi-coordinated one and they could be formed only in small amounts as experimentally observed.

However, a stronger destabilization of the interaction is observed due to the solvation process. This destabilization effect is related to the hydration energy of the acids and to the solvation-desolvation process of the acid and the surface.

Moreover, the explicit solvent modifies the first interaction between the acid and the surface. In water, in all three pH conditions, acid molecules interact with the hydrated surface as a mono-negative charge species due to the proton transfer, before grafting.

Likewise, gas-phase calculations, the most stable interactions show a bi-dentate coordination. The two species involved are the result of a bi-dissociated process in neutral conditions and a mono-dissociated process in anionic conditions. However, the most negative IE$_{w\_2}$ value is reported for di-anionic acid and shows a stable tri-coordinated structures. However, this conformation can be formed only in small amount with respect to bi-coordinated ones.

Therefore, the formation of di-anionic acid species, due to a PT process or a change in pH, favors the anchoring of alkylphosphonic acid to rutile TiO$_2$ (1 1 0).

CRediT authorship contribution statement

Daniele Veclani: Methodology, Formal analysis, Validation, Investigation, Writing – original draft, Visualization. **Andrea Melchior:** Methodology, Writing – review & editing. **Antoni Llobet:**
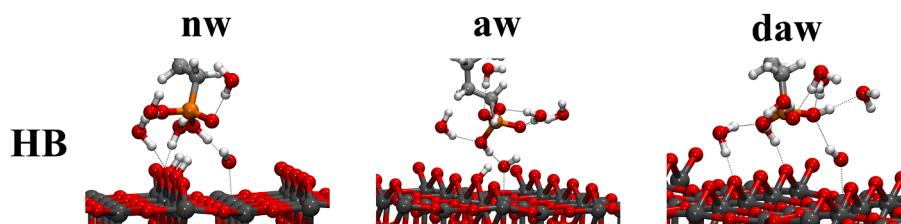
Fig. 6. Optimized HB structures for neutral-C12-PA (nw), anionic-C12-PA (aw) and dianionic-C12-PA (daw) in water. Proton transfer process take place before the formation of the bond between the acid and the surface.

Conceptualization, Writing – review & editing, Funding acquisition. **Nicola Armaroli:** Conceptualization, Writing – review & editing, Funding acquisition. **Alessandro Venturini:** Methodology, Writing – review & editing, Formal analysis, Visualization, Supervision.

Declaration of Competing Interest

The authors declare that they have no known competing financial interests or personal relationships that could have appeared to influence the work reported in this paper.

Data availability

Data will be made available on request.

Data Availability Statement

The raw/processed data required to reproduce these findings cannot be shared at this time as the data also forms part of an ongoing study.

Appendix A. Supplementary material

Supplementary data to this article can be found online at https://doi.org/10.1016/j.commatsci.2022.111997.

References

[1] T. Biswal, S.K. BadJena, D. Pradhan, Sustainable biomaterials and their applications: A short review, Mater. Today: Proc. 30 (2020) 274–282, https://doi.org/10.1016/j.matpr.2020.01.437.

[2] A.J. Festas, A. Ramos, J.P. Davim, Medical devices biomaterials – A review, Proc. Inst. Mech. Eng. Pt. L J. Mater. Des. Appl. 234 (2020) 218–228. https://doi.org/10.1177/1464420719882458.

[3] M. Kaur, K. Singh, Review on titanium and titanium based alloys as biomaterials for orthopaedic applications, Mater. Sci. Eng. C 102 (2019) 844–862, https://doi.org/10.1016/j.msec.2019.04.064.

[4] M. Niinomi, M. Nakai, J. Hieda, Development of new metallic alloys for biomedical applications, Acta Biomater. 8 (2012) 3888–3903, https://doi.org/10.1016/j.actbio.2012.06.037.

[5] D. Annur, I. Kartika, S. Supriadi, B. Suharno, Titanium and titanium based alloy prepared by spark plasma sintering method for biomedical implant applications - A review, Mater. Res. Express. 8 (2021) 012001, https://doi.org/10.1088/2053-1591/abd969.

[6] J.W. Nicholson, Titanium Alloys for Dental Implants: A Review, Prosthesis. 2 (2020) 100–116, https://doi.org/10.3390/prosthesis2020011.

[7] G. De Cicco, D. Tosi, R. Crisci, A. Bortolami, T.M. Aquino, A. Prencipe, G. Di Matteo, S. Benussi, Use of new cannulated screws for primary sternal closure in high risk patients for sternal dehiscence, J. Thorac. Dis. 11 (2019) 4538–4543, https://doi.org/10.21037/jtd.2019.10.79.

[8] B. Ladd, D. Polly, Pelvic Fixation Using S2AI and Triangular Titanium Implants (Bedrock Technique), World Neurosurg. 154 (2021) 2, https://doi.org/10.1016/j.wneu.2021.07.027.

[9] Y. Mohammed, K. Zhang, H. Baumgart, A.A. Elmustafa, Investigation of the Nanomechanical Properties of Titanium Oxide Films Synthesized Using Atomic Layer Deposition, ECS, Meeting Abstracts. MA2018-02 (2018) 700, https://doi.org/10.1149/ma2018-02/16/700.

[10] A. Ravoiu, L. Benea, A. Chiriac, Metabolic Albumin and Its Effect on Electrochemical Behavior of Titanium Implant Alloy, IOP Conf. Ser.: Mater. Sci. Eng. 374 (2018), 012077, https://doi.org/10.1088/1757-899X/374/1/012077.

[11] H. Chouirfa, H. Bouloussa, V. Migonney, C. Falentin-Daudré, Review of titanium surface modification techniques and coatings for antibacterial applications, Acta Biomater. 83 (2019) 37–54, https://doi.org/10.1016/j.actbio.2018.10.036.

[12] X. Liu, P.K. Chu, C. Ding, Surface modification of titanium, titanium alloys, and related materials for biomedical applications, Mater. Sci. Eng. R Rep. 47 (2004) 49–121, https://doi.org/10.1016/j.mser.2004.11.001.

[13] J. Sharan, S.V. Lale, V. Koul, M. Mishra, O.P. Kharbanda, An Overview of Surface Modifications of Titanium and its Alloys for Biomedical Applications, Trends Biomater, Artif. Organs. 29 (2015) 176–187.

[14] D. Campoccia, L. Montanaro, C.R. Arciola, A review of the biomaterials technologies for infection-resistant surfaces, Biomaterials. 34 (2013) 8533–8554, https://doi.org/10.1016/j.biomaterials.2013.07.089.

[15] L. Zhou, Y. Lai, W. Huang, S. Huang, Z. Xu, J. Chen, D. Wu, Biofunctionalization of microgroove titanium surfaces with an antimicrobial peptide to enhance their bactericidal activity and cytocompatibility, Colloids Surf B Biointerfaces. 128 (2015) 552–560, https://doi.org/10.1016/j.colsurfb.2015.03.008.

[16] H. Davidson, M. Poon, R. Saunders, I.M. Shapiro, N.J. Hickok, C.S. Adams, Tetracycline tethered to titanium inhibits colonization by Gram-negative bacteria, J. Biomed. Mater. Res. B Appl. Biomater. 103 (2015) 1381–1389, https://doi.org/10.1002/jbm.b.33310.

[17] S.J. Lee, D.N. Heo, H.R. Lee, D. Lee, S.J. Yu, S.A. Park, W.K. Ko, S.W. Park, S.G. Im, J.H. Moon, I.K. Kwon, Biofunctionalized titanium with anti-fouling resistance by grafting thermo-responsive polymer brushes for the prevention of peri-implantitis, J. Mater. Chem. B. 3 (2015) 5161–5165, https://doi.org/10.1039/c5tb00611b.

[18] H. Chouirfa, M.D.M. Evans, D.G. Castner, P. Bean, D. Mercier, A. Galtayries, C. Falentin-Daudré, V. Migonney, Grafting of architecture controlled poly(styrene sodium sulfonate) onto titanium surfaces using bio-adhesive molecules: Surface characterization and biological properties, Biointerphases. 12 (2017) 02C418, https://doi.org/10.1116/1.4985608.

[19] R. Chen, M.D.P. Willcox, K.K.K. Ho, D. Smyth, N. Kumar, Antimicrobial peptide melimine coating for titanium and its in vivo antibacterial activity in rodent subcutaneous infection models, Biomaterials. 85 (2016) 142–151, https://doi.org/10.1016/j.biomaterials.2016.01.063.

[20] E. Gerits, S. Kucharíková, P. Van Dijck, M. Erdtmann, A. Krona, M. Lövenklev, M. Fröhlich, B. Dovgan, F. Impellizzeri, A. Braem, J. Vleugels, S.C.A. Robijns, H. P. Steenackers, J. Vanderleyden, K. De Brucker, K. Thevissen, B.P.A. Cammue, M. Fauvart, N. Verstraeten, J. Michiels, Antibacterial activity of a new broad-spectrum antibiotic covalently bound to titanium surfaces, J. Orthop. 34 (2016) 2191–2198, https://doi.org/10.1002/jor.23238.

[21] Y.G. Aronoff, B. Chen, G. Lu, C. Seto, J. Schwartz, S.L. Bernasek, Stabilization of Self-Assembled Monolayers of Carboxylic Acids on Native Oxides of Metals, J. Am. Chem. Soc. 119 (1997) 259–262, https://doi.org/10.1021/ja953848+.

[22] P. Canepa, G. Gonella, G. Pinto, V. Grachev, M. Canepa, O. Cavalleri, Anchoring of Aminophosphonates on Titanium Oxide for Biomolecular Coupling, J. Phys. Chem. C. 123 (2019) 16843–16850, https://doi.org/10.1021/acs.jpcc.9b04077.

[23] J. Peyre, V. Humblot, C. Méthivier, J.M. Berjeaud, C.M. Pradier, Co-grafting of amino-poly(ethylene glycol) and Magainin I on a TiO$_2$ surface: Tests of antifouling and antibacterial activities, J. Phys. Chem. B. 116 (2012) 13839–13847, https://doi.org/10.1021/jp305597y.

[24] C. Pereira, J.S. Baumann, P. Masson, G. Pourroy, A. Carradò, V. Migonney, C. Falentin-Daudre, Double Functionalization for the Design of Innovative Craniofacial Prostheses, JOM. 74 (2022) 87–95, https://doi.org/10.1007/s11837-021-04997-0.

[25] C. Tudisco, V. Oliveri, M. Cantarella, G. Vecchio, G.G. Condorelli, Cyclodextrin anchoring on magnetic Fe$_3$O$_4$ nanoparticles modified with phosphonic linkers, Eur. J. Inorg Chem. (2012) 5323–5331, https://doi.org/10.1002/ejic.201200510.

[26] G.A. Seisenbaeva, I.V. Melnyk, N. Hedin, Y. Chen, P. Eriksson, E. Trzop, Y.L. Zub, V.G. Kessler, Molecular insight into the mode-of-action of phosphonate monolayers as active functions of hybrid metal oxide adsorbents. Case study in sequestration of rare earth elements, RSC Adv. 5 (2015) 24575–24585, https://doi.org/10.1039/c4ra15531a.

[27] B. Zhang, J.N.H. Reek, Supramolecular Strategies for the Recycling of Homogeneous Catalysts, Chem. Asian J. 16 (2021) 3851–3863, https://doi.org/10.1002/asia.202100968.

[28] L. Azizova, D. Morgan, J. Rowlands, E. Brousseau, T. Kulik, B. Palianytsia, J. P. Mansell, J. Birchall, T. Wilkinson, A. Sloan, W.N. Ayre, Parameters controlling octadecyl phosphonic acid self-assembled monolayers on titanium dioxide for anti-fouling biomedical applications, Appl. Surf. Sci. 604 (2022), 154462, https://doi.org/10.1016/j.apsusc.2022.154462.

[29] P. Bhanja, J. Na, T. Jing, J. Lin, T. Wakihara, A. Bhaumik, Y. Yamauchi, Nanoarchitectured Metal Phosphates and Phosphonates: A New Material Horizon toward Emerging Applications, Chem. Mater. 31 (2019) 5343–5362, https://doi.org/10.1021/acs.chemmater.9b01742.

[30] L. Zeininger, L. Portilla, M. Halik, A. Hirsch, Quantitative Determination and Comparison of the Surface Binding of Phosphonic Acid, Carboxylic Acid, and Catechol Ligands on TiO$_2$ Nanoparticles, Eur. J. Chem. 22 (2016) 13506–13512, https://doi.org/10.1002/chem.201601920.

[31] M. Wagstaffe, A.G. Thomas, M.J. Jackman, M. Torres-Molina, K.L. Syres, K. Handrup, An experimental investigation of the adsorption of a phosphonic acid on the anatase TiO$_2$(101) surface, J. Phys. Chem. C. 120 (2016) 1693–1700, https://doi.org/10.1021/acs.jpcc.5b11258.

[32] E.S. Skibinski, W.J.I. DeBenedetti, M.A. Hines, Solution Deposition of Phenylphosphinic Acid Leads to Highly Ordered, Covalently Bound Monolayers on TiO$_2$(110) Without Annealing, J. Phys. Chem. C. 121 (2017) 14213–14221, https://doi.org/10.1021/acs.jpcc.7b04167.

[33] L. Sang, K.M. Knesting, A. Bulusu, A.K. Sigdel, A.J. Giordano, S.R. Marder, J. J. Berry, S. Graham, D.S. Ginger, J.E. Pemberton, Effect of time and deposition method on quality of phosphonic acid modifier self-assembled monolayers on indium zinc oxide, Appl. Surf. Sci. 389 (2016) 190–198, https://doi.org/10.1016/j.apsusc.2016.06.183.

[34] V. Lafond, C. Gervais, J. Maquet, D. Prochnow, F. Babonneau, P.H. Mutin, ^{17}O MAS NMR Study of the Bonding Mode of Phosphonate Coupling Molecules in a Titanium

Oxo-Alkoxo-Phosphonate and in Titania-Based Hybrid Materials, Chem. Mater. 15 (2003) 4098–4103, https://doi.org/10.1021/cm031061+.

[35] G. Guerrero, P.H. Mutin, A. Vioux, Anchoring of phosphonate and phosphinate coupling molecules on titania particles, Chem. Mater. 13 (2001) 4367–4373, https://doi.org/10.1021/cm001253u.

[36] G. Guerrero, J.G. Alauzun, M. Granier, D. Laurencin, P.H. Mutin, Phosphonate coupling molecules for the control of surface/interface properties and the synthesis of nanomaterials, Dalton Trans. 42 (2013) 12569–12585, https://doi.org/10.1039/c3dt51193f.

[37] W. Gao, L. Dickinson, C. Grozinger, F.G. Morin, L. Reven, Self-Assembled Monolayers of Alkylphosphonic Acids on Metal Oxides, Langmuir. 12 (1996) 6429–6435. https://pubs.acs.org/sharingguidelines.

[38] J.M. Ferreira, S. Marcinko, R. Sheardy, A.Y. Fadeev, Calorimetric study of the reactions of n-alkylphosphonic acids with metal oxide surfaces, J Colloid Interface Sci. 286 (2005) 258–262, https://doi.org/10.1016/j.jcis.2004.11.008.

[39] F. Brodard-Severac, G. Guerrero, J. Maquet, P. Florian, C. Gervais, P.H. Mutin, High-field ^{17}O MAS NMR investigation of phosphonic acid monolayers on titania, Chem. Mater. 20 (2008) 5191–5196, https://doi.org/10.1021/cm8012683.

[40] R. Boissezon, J. Muller, V. Beaugeard, S. Monge, J.J. Robin, Organophosphonates as anchoring agents onto metal oxide-based materials: Synthesis and applications, RSC Advances. 4 (2014) 35690–35707, https://doi.org/10.1039/c4ra05414h.

[41] S. Farquharson, A. Gift, P. Maksymiuk, F.E. Inscore, W.W. Smith, pH dependence of methyl phosphonic acid, dipicolinic acid, and cyanide by surface-enhanced Raman spectroscopy, Proc. SPIE 5269, Chemical and Biological Point Sensors for Homeland Defense. 5269 (2004) 117. https://doi.org/10.1117/12.510626.

[42] Y.C. Quintero, R. Nagarajan, Molecular and dissociative adsorption of DMMP, Sarin and Soman on dry and wet TiO$_2$(110) using density functional theory, Surf Sci. 675 (2018) 26–35, https://doi.org/10.1016/j.susc.2018.04.002.

[43] C.L. Pang, M. Watkins, G. Cabailh, S. Ferrero, L.T. Ngo, Q. Chen, D.S. Humphrey, A. L. Shluger, G. Thornton, Bonding of methyl phosphonate to TiO$_2$(110), J. Phys. Chem. C. 114 (2010) 16983–16988, https://doi.org/10.1021/jp1018923.

[44] M. Nilsing, S. Lunell, P. Persson, L. Ojamäe, Phosphonic acid adsorption at the TiO$_2$ anatase (101) surface investigated by periodic hybrid HF-DFT computations, Surf. Sci. 582 (2005) 49–60, https://doi.org/10.1016/j.susc.2005.02.044.

[45] R. Luschtinetz, J. Frenzel, T. Milek, G. Seifert, Adsorption of phosphonic acid at the TiO$_2$ anatase (101) and rutile (110) surfaces, J. Phys. Chem. C. 113 (2009) 5730–5740, https://doi.org/10.1021/jp8110343.

[46] N. Gys, L. Siemons, B. Pawlak, K. Wyns, K. Baert, T. Hauffman, P. Adriaensens, F. Blockhuys, B. Michielsen, S. Mullens, V. Meynen, Experimental and computational insights into the aminopropylphosphonic acid modification of mesoporous TiO$_2$ powder: The role of the amine functionality on the surface interaction and coordination, Appl Surf Sci. 566 (2021), 150625, https://doi.org/10.1016/j.apsusc.2021.150625.

[47] C. Di Costa, D. Costa, Anatase TiO$_2$ surface functionalization by alkylphosphonic acid: A DFT+D study, J. Phys. Chem. C. 116 (2012) 2819–2828, https://doi.org/10.1021/jp203256s.

[48] V.M. Bermudez, Ab initio study of the interaction of dimethyl methylphosphonate with rutile (110) and anatase (101) TiO$_2$ surfaces, J. Phys. Chem. C. 114 (2010) 3063–3074, https://doi.org/10.1021/jp9098304.

[49] J.G. Van Dijck, H. Lenaerts, L. Siemons, F. Blockhuys, V. Meynen, The interaction of water with organophosphonic acid surface modified titania: An in-depth in-situ DRIFT study, Surf. Interfaces. 21 (2020), 100710, https://doi.org/10.1016/j.surfin.2020.100710.

[50] Y. Chen, E. Trzop, J.D. Sokolow, P. Coppens, Direct observation of the binding mode of the phosphonate anchor to nanosized polyoxotitanate clusters, Eur. J. Chem. 19 (2013) 16651–16655, https://doi.org/10.1002/chem.201302012.

[51] M. Kurban, B. Gündüz, Physical and optical properties of DCJTB dye for OLED display applications, Experimental and theoretical investigation, J Mol Struct. 1137 (2017) 403–411, https://doi.org/10.1016/j.molstruc.2017.02.064.

[52] M. Kurban, B. Gündüz, F. Göktaş, Experimental and theoretical studies of the structural, electronic and optical properties of BCzVB organic material, Optik (Stuttg) 182 (2019) 611–617, https://doi.org/10.1016/j.ijleo.2019.01.080.

[53] Y. Liu, R.-J. Gou, S.-H. Zhang, Y.-H. Chen, H.J. Cheng, M.-H. Chen, Solvent effect on the formation of NTO/TZTN cocrystal explosives, Comput Mater Sci. 163 (2019) 308–314, https://doi.org/10.1016/j.commatsci.2019.03.035.

[54] B. Aradi, B. Hourahine, T. Frauenheim, DFTB+, a sparse matrix-based implementation of the DFTB method, J. Phys. Chem. A. 111 (2007) 5678–5684, https://doi.org/10.1021/jp070186p.

[55] M. Elstner, The SCC-DFTB method and its application to biological systems, Theor Chem Acc. 116 (2006) 316–325, https://doi.org/10.1007/s00214-005-0066-0.

[56] F. Spiegelman, N. Tarrat, J. Cuny, L. Dontot, E. Posenitskiy, C. Martí, A. Simon, M. Rapacioli, Density-functional tight-binding: basic concepts and applications to molecules and clusters, ADV PHYS-X. 5 (2019) 1710252, https://doi.org/10.1080/23746149.2019.1710252.

[57] F. Balzaretti, V. Gupta, L.C. Ciacchi, B. Aradi, T. Frauenheim, S. Köppen, Water Reactions on Reconstructed Rutile TiO2: A Density Functional Theory/Density Functional Tight Binding Approach, J. Phys. Chem. C. 125 (2021) 13234–13246, https://doi.org/10.1021/acs.jpcc.1c00871.

[58] D. Selli, G. Fazio, C. Di Valentin, Using density functional theory to model realistic TiO$_2$ nanoparticles, their photoactivation and interaction with water, Catalysts. 7 (2017) 357, https://doi.org/10.3390/catal7120357.

[59] D. Selli, G. Fazio, G. Seifert, C. Di Valentin, Water Multilayers on TiO$_2$ (101) Anatase Surface: Assessment of a DFTB-Based Method, J Chem Theory Comput. 13 (2017) 3862–3873, https://doi.org/10.1021/acs.jctc.7b00479.

[60] S. Manzhos, G. Giorgi, K. Yamashita, A density functional tight binding study of acetic acid adsorption on crystalline and amorphous surfaces of titania, Molecules. 20 (2015) 3371–3388, https://doi.org/10.3390/molecules20023371.

[61] V.S. Naumov, A.S. Loginova, A.A. Avdoshin, S.K. Ignatov, A.V. Mayorov, B. Aradi, T. Frauenheim, Structural, electronic, and thermodynamic properties of TiO$_2$/organic clusters: performance of DFTB method with different parameter sets, Int J Quantum Chem. 121 (2021) 1–19, https://doi.org/10.1002/qua.26427.

[62] C. Ronchi, M. Datteo, M. Kaviani, D. Selli, C. Di Valentin, Unraveling Dynamical and Light Effects on Functionalized Titanium Dioxide Nanoparticles for Bioconjugation, J. Phys. Chem. C. 123 (2019) 10130–10144, https://doi.org/10.1021/acs.jpcc.9b01385.

[63] B. Hourahine, B. Aradi, V. Blum, F. Bonafé, A. Buccheri, C. Camacho, C. Cevallos, M.Y. Deshaye, T. Dumitric, A. Dominguez, S. Ehlert, M. Elstner, T. Van Der Heide, J. Hermann, S. Irle, J.J. Kranz, C. Köhler, T. Kowalczyk, T. Kubar, I.S. Lee, V. Lutsker, R.J. Maurer, S.K. Min, I. Mitchell, C. Negre, T.A. Niehaus, A.M.N. Niklasson, A.J. Page, A. Pecchia, G. Penazzi, M.P. Persson, J. Åtild, ezáč, C.G. Sánchez, M. Sternberg, M. Stöhr, F. Stuckenberg, A. Tkatchenko, V.W.Z. Yu, T. Frauenheim, DFTB+, a software package for efficient approximate density functional theory based atomistic simulations, Chem. Phys. 152 (2020) 124101. https://doi.org/10.1063/1.5143190.

[64] L. Guimarães, A.N. Enyashin, J. Frenzel, T. Heine, H.A. Duarte, G. Seifert, Imogolite Nanotubes: Stability, Electronic, and Mechanical Properties, ACS Nano. 1 (2007) 362–368.

[65] E. Caldeweyher, S. Ehlert, A. Hansen, H. Neugebauer, S. Spicher, C. Bannwarth, S. Grimme, A generally applicable atomic-charge dependent London dispersion correction, J. Phys. Chem. C. 114 (2019), 161415, https://doi.org/10.1016/0022-3913(83)90359-1.

[66] C. Lun Pang, R. Lindsay, G. Thornton, Chemical reactions on rutile TiO$_2$(110), Chem. Soc. Rev. 37 (2008) 2328–2353, https://doi.org/10.1039/b719085a.

[67] G.J. Martyna, M.E. Tuckerman, D.J. Tobias, M.L. Klein, Explicit reversible integrators for extended systems dynamics, Mol. Phys. 87 (1996) 1117–1157, https://doi.org/10.1080/00268979600100761.

[68] C.E. Housecroft, H.D. Brooke Jenkins, Absolute ion hydration enthalpies and the role of volume within hydration thermodynamics, RSC Adv. 7 (2017) 27881–27894, https://doi.org/10.1039/c6ra25804b.

[69] D. Reyes-Coronado, G. Rodríguez-Gattorno, M.E. Espinosa-Pesqueira, C. Cab, R. De Coss, G. Oskam, Phase-pure TiO$_2$ nanoparticles: Anatase, brookite and rutile, Nanotechnology. 19 (2008), https://doi.org/10.1088/0957-4484/19/14/145605.

[70] S. Manzhos, Comparative density functional theory and density functional tight binding study of 2-anthroic acid on TiO$_2$, Chem. Phys. Lett. 643 (2016) 16–20, https://doi.org/10.1016/j.cplett.2015.11.007.

[71] N. Martsinovich, D.R. Jones, A. Troisi, Electronic structure of TiO$_2$ surfaces and effect of molecular adsorbates using different DFT implementations, J. Phys. Chem. C. 114 (2010) 22659–22670, https://doi.org/10.1021/jp109756g.

[72] G. Dolgonos, B. Aradi, N.H. Moreira, T. Frauenheim, An improved self-consistent-charge density-functional tight-binding (SCC-DFTB) set of parameters for simulation of bulk and molecular systems involving titanium, J. Chem. Theory Comput. 6 (2010) 266–278, https://doi.org/10.1021/ct900422c.